universe

MDPI

Article

Spin-Charge-Induced Scalarization of Kerr–Newman Black Holes in the Einstein–Maxwell-Scalar Theory with Scalar Potential

Xiang Luo [1], Meng-Yun Lai [1], Yun Soo Myung [2], Yi-Bin Huang [1] and De-Cheng Zou [1,*]

[1] College of Physics and Communication Electronics, Jiangxi Normal University, Nanchang 330022, China; lx32000@163.com (X.L.); mengyunlai@jxnu.edu.cn (M.-Y.L.); huangyb31@aliyun.com (Y.-B.H.)
[2] Center for Quantum Spacetime, Sogang University, Seoul 04107, Republic of Korea; ysmyung@inje.ac.kr
* Correspondence: dczou@jxnu.edu.cn

Abstract

We investigate the spin-charge-induced scalarization of Kerr–Newman (KN) black holes in the Einstein–Maxwell-scalar (EMS) theory with a scalar potential and positive coupling parameter. In the linearized theory, there exists a bound of $0 < a < a_o$ with onset spin a_c for the negative region signaling instability by analyzing the effective scalar mass term in the θ-direction. Solving the $(2+1)$-dimensional evolution equation numerically, we find the region where the KN black hole becomes unstable, giving rise to scalarized KN black holes. The threshold curve for representing the boundary between stable and unstable KN black holes depends on charge Q, scalar mass m_ϕ, coupling parameter α, and spin parameter a with upper bound $a^2 \leq M^2 - Q^2$.

Keywords: scalarization; Einstein–Maxwell-scalar theory; Kerr–Newman black holes

1. Introduction

The no-hair theorem has long shaped black hole physics in general relativity, stating that mass (M), charge (Q), and spin ($a = J/M$) with J angular momentum describe Kerr–Newman (KN) black holes [1,2]. It rules out regular scalar solutions in flat spacetimes because scalar fields become unstable and blow up at the horizon [3–5]. In 1993, however, Damour and Esposito-Farèse found a new way of avoiding this theorem by making use of scalar–tensor theories with special scalar couplings. They showed that scalar hair could survive on black holes without breaking physics [6]. The breakthrough came out when theorists probed two specific models. In scalar–tensor theories that include the nonminimal scalar coupling to either the Gauss–Bonnet (GB) term [7–9] or Maxwell term [10–13], the scalar field triggered destabilization of bald (scalar-free) black holes and induced scalarized (charged) black holes. That is, the tachyonic scalar played an important role in triggering spontaneous scalarization of the bald black holes.

Recent works have shown that in scalar-Gauss–Bonnet gravity, scalarization of Kerr black holes depends on spin a and coupling parameter. For a negative coupling parameter, scalarization is allowed when spin exceeds $a \geq 0.5M$, as confirmed by studies [14–17]. In this direction, high rotation triggered tachyonic instability [18], and it was validated numerically [19–21]. Analyses using different coupling functions [22,23] further confirmed that scalarization depends on both spin and coupling parameter. We remind the reader that the spin-induced scalarization of a Kerr black hole with a massive scalar were also discussed in scalar-Gauss–Bonnet theory [24] and dynamical Chern–Simons gravity [25].

Check for updates

Academic Editor: Júlio César Fabris

Received: 27 January 2026
Revised: 3 March 2026
Accepted: 11 March 2026
Published: 16 March 2026

Copyright: © 2026 by the authors. Licensee MDPI, Basel, Switzerland. This article is an open access article distributed under the terms and conditions of the Creative Commons Attribution (CC BY) license.

In the Einstein–Maxwell-scalar (EMs) theory with scalar coupling parameter α, scalarization for KN black holes has also been investigated. The threshold curves $[\alpha(a)]$ were found with a different charge Q, describing the boundary between KN and scalarized KN black holes in the EMS theory. For negative coupling parameter, a lower bound of $\frac{a}{r_+} \geq \hat{a}(= 0.4142)$ was found in the limit of $\alpha \to -\infty$ by using analytical [26] and two numerical [27] methods—the hyperboloidal foliation time evolution method [28] and the direct 2 + 1 time evolution method. For the positive coupling parameter, however, there was no lower bound on a, while the upper bound of a ($a^2 \leq M^2 - Q^2$) appeared as the existence condition for the outer horizon [29]. This implies that the high rotation enhances scalarization for KN black holes in EMs theory.

In the present work, we wish to study the spin-charge-induced scalarization of a KN black hole when the scalar field is massive and the scalar coupling parameter is positive $\alpha > 0$. We will adopt the direct 2 + 1 time evolution method [24,25] to perform a time evolution of linearized massive scalar perturbation on the KN black hole background. In this case, we expect to find that the scalar mass term might alter tachyonic instability and spin-charge-induced scalarization significantly.

We organize the present work as follows. In Section 2, we revisit the linearized scalar theory by analyzing the effective scalar mass term $\mu^2_{\rm eff}$. We perform the spin-charge-induced scalarization of KN black holes in Section 3 by solving the (2 + 1)-dimensional evolution equation numerically and then show the numerical results for different parameters Q, α, a, etc., in Section 4. Section 5 is devoted to contributing to conclusions and discussions.

2. Linearized Scalar Theory

The action of EMS theory with scalar potential takes the form [12,30]

$$S_{\rm EMS} = \frac{1}{16\pi}\int d^4x\sqrt{-g}\Big[R - 2\partial_\mu\phi\partial^\mu\phi - U(\phi) - f(\phi)F^2\Big], \tag{1}$$

where R is the Ricci scalar, ϕ is the scalar field with a potential $U(\phi)$, and the scalar coupling function $f(\phi)$ is coupled to the Maxwell term $F^2 = F_{\mu\nu}F^{\mu\nu}$ with $F_{\mu\nu} = \partial_\mu A_\nu - \partial_\nu A_\mu$.

The variation of action (1) with respect to the metric $g_{\mu\nu}$, scalar field ϕ, and vector potential A_μ gives the following equations:

$$R_{\mu\nu} - \frac{1}{2}Rg_{\mu\nu} = 2\partial_\mu\phi\partial_\nu\phi - (\partial\phi)^2 g_{\mu\nu} + 2f(\phi)\Big(F_{\mu\rho}F_\nu{}^\rho - \frac{F^2}{4}g_{\mu\nu}\Big), \tag{2}$$

$$\nabla_\mu\nabla^\mu\phi - \frac{1}{4}f'(\phi)F^2 - \frac{1}{4}U'(\phi) = 0, \tag{3}$$

$$\partial_\mu\big(\sqrt{-g}f(\phi)F^{\mu\nu}\big) = 0, \tag{4}$$

where the prime ($'$) denotes the derivative with respect to its argument.

Without scalar hair, the axisymmetric KN black hole solution is expressed in terms of the Boyer–Lindquist coordinates as

$$\begin{aligned} ds^2_{\rm KN} \equiv \bar{g}_{\mu\nu}dx^\mu dx^\nu &= -\frac{\Delta - a^2\sin^2\theta}{\rho^2}dt^2 - \frac{2a\sin^2\theta(r^2+a^2-\Delta)}{\rho^2}dtd\varphi \\ &+ \frac{[(r^2+a^2)^2 - \Delta a^2\sin^2\theta]\sin^2\theta}{\rho^2}d\varphi^2 + \frac{\rho^2}{\Delta}dr^2 + \rho^2 d\theta^2, \end{aligned} \tag{5}$$

where

$$\Delta = r^2 - 2Mr + a^2 + Q^2, \quad \rho^2 = r^2 + a^2\cos^2\theta.$$

The corresponding vector potential is given by

$$A = -\frac{Qr}{\rho^2}\Big(dt - a\sin^2\theta d\varphi\Big). \tag{6}$$

The outer and inner horizons are obtained by imposing $\Delta = (r - r_+)(r - r_-) = 0$ as

$$r_\pm = M \pm \sqrt{M^2 - a^2 - Q^2}, \tag{7}$$

where one requires the existence condition for two horizons with $M \geq Q$

$$a^2 \leq M^2 - Q^2 \tag{8}$$

For simplicity, we set the mass of the KN black hole to be $M = 1$ in the whole article.

To handle the tachyonic instability of KN black holes in the EMS theory, we consider the linearized scalar equation

$$\Big(\bar{\Box} - \mu^2_{\text{eff}}\Big)\delta\phi = 0, \quad \mu^2_{\text{eff}} = \frac{1}{4}\Big[\bar{F}^2 f''(0) + U''(0)\Big]. \tag{9}$$

This instability is characterized by the presence of a negative mass term ($\mu^2_{\text{eff}} < 0$) in the linearized scalar equation. Until now, many authors adopted different forms of the coupling function $f(\phi)$ with coupling parameter α, exponential form ($e^{\alpha\phi^2}$) [12], quadratic form ($1 + \alpha\phi^2$) [13], and hyperbolic cosine form ($\cosh[\sqrt{2\alpha}\phi]$) [10]. We introduce an interesting potential function as $U(\phi)$= $m^2_\phi\phi^2$ with m^2_ϕ mass of the scalar, as shown in Ref. [30]. Without loss of generality, we do not choose any specific form of coupling function $f(\phi)$ but require that $f(\phi)$ satisfies [10,11]

$$f(0) = 1, \quad f'(0) = 0, \quad f''(0) = 2\alpha, \tag{10}$$

where $f(0) = 1$ implies the presence of the Maxwell term even for non-scalar coupling, $f'(0) = 0$ denotes the presence of a scalar coupling function, and the last $f''(0) = 2\alpha$ means the presence of a quadratic scalar function with coupling parameter α. For the KN black hole background, the effective mass squared in Equation (9) is given by

$$\mu^2_{\text{eff}} = \frac{\alpha\bar{F}^2}{2} + \frac{1}{2}m^2_\phi = -\frac{\alpha Q^2(r^4 - 6a^2r^2\cos^2\theta + a^4\cos^4\theta)}{(r^2 + a^2\cos^2\theta)^4} + \frac{1}{2}m^2_\phi. \tag{11}$$

Intuitively, the influence of μ^2_{eff} on the tachyonic instability could be found in the near-horizon if one chooses θ appropriately. For $\theta = \pi/2$, its spin (a) dependence disappears, but its contribution is dominant. Hence, we may choose $\theta = 0, \frac{\pi}{3}, \frac{0.9\pi}{2}$ to obtain its simple spin dependence. In this case, we find the bound for scalarization with positive α as

$$0 < a < a_o(Q, m_\phi, \alpha), \tag{12}$$

where a_o denotes the onset spin, depending on three parameters of Q, m_ϕ, and α.

One observes from Figure 1 with $Q = 0.6$ and $\alpha = 24$ the appearance of a negative region for $\mu^2_{\text{eff}}|_{\theta=0}$ in the near-horizon: $0 < a < a_o(= 0.5509)$. However, for $\theta = \frac{\pi}{3}, \frac{0.9\pi}{2}$, there are no onset spins. We observe from Figure 2 with $Q = 0.4$ and $\alpha = 65$ the appearance of negative regions for $\mu^2_{\text{eff}}|_{\theta=0,\frac{\pi}{3}}$ in the near-horizon: $0 < a < a_o(= 0.5818)$ and $0 < a < a_o(= 0.9062)$. However, for $\theta = \frac{0.9\pi}{2}$, there is no onset spin. This implies that as a whole, there is no spin-bound on the onset of scalarization with positive coupling parameter α because the contribution of μ^2_{eff} around ($\theta = \pi/2$) is dominant negatively.

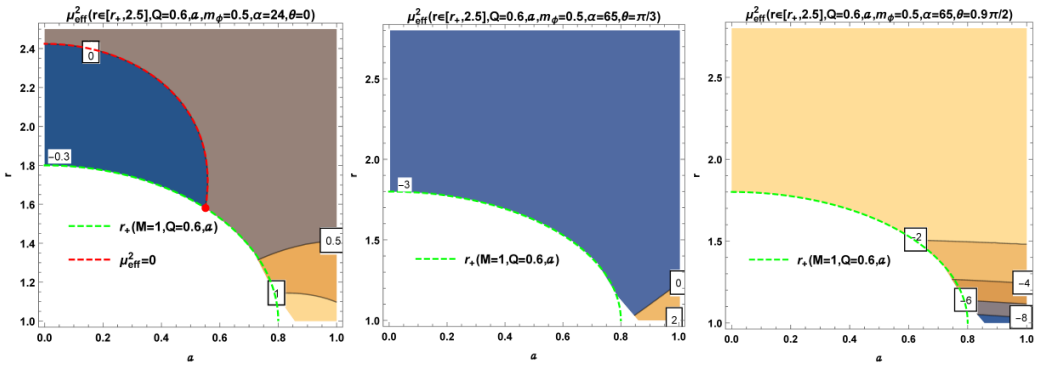

(**a**) $Q = 0.6$, $\theta = 0$ (**b**) $Q = 0.6$, $\theta = \frac{\pi}{3}$ (**c**) $Q = 0.6$, $\theta = \frac{0.9\,\pi}{2}$

Figure 1. Contour graphs for showing the sign change of $\mu^2_{\rm eff}(r \in [r_+, 2.5], Q = 0.6, a \in [0, 1], m_\phi = 0.5, \alpha = 24, \theta)$ as functions of r and spin a with three different θ. Here, $\mu^2_{\rm eff} = 0$ represents its zero value (red-dashed curve) and $r_+(M = 1, Q = 0.6, a \in [0, 0.8])$ denotes the horizon radius (green-dashed curve). The different shaded regions correspond to their different $\mu^2_{\rm eff}$ values between boundary curves. (**a**) $\theta = 0$. One finds that the negative region is given by $0 < a < a_o$(=0.5509, red dot). (**b**) $\theta = \frac{\pi}{3}$. One finds the whole negative region in the near-horizon. (**c**) $\theta = \frac{0.9\pi}{2}$. The whole negative region is found in the near-horizon.

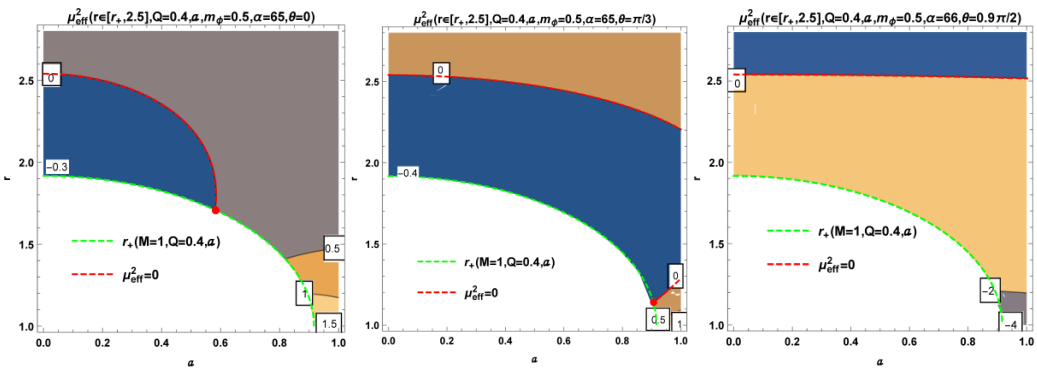

(**a**) $Q = 0.4$, $\theta = 0$ (**b**) $Q = 0.4$, $\theta = \frac{\pi}{3}$ (**c**) $Q = 0.4$, $\theta = \frac{0.9\,\pi}{2}$

Figure 2. Contour graphs for showing the sign change of $\mu^2_{\rm eff}(r \in [r_+, 2.5], Q = 0.4, a \in [0, 1], m_\phi = 0.5, \alpha = 65, \theta)$ as functions of r and spin a with three different θ. Here, $\mu^2_{\rm eff} = 0$ represents its zero curve (red-dashed) and $r_+(M = 1, Q = 0.4, a \in [0, 0.917])$ denotes the horizon radius (green-dashed). (**a**) $\theta = 0$. One finds that the negative region is allowed for $0 < a < a_o$(=0.5818, red dot). (**b**) $\theta = \frac{\pi}{3}$. One finds that the negative region is given by $0 < a < a_o$(=0.9062, red dot). (**c**) $\theta = \frac{0.9\pi}{2}$. One finds the whole negative region in the near-horizon.

3. Spin-Charge-Induced Scalarization

We adopt the numerical method to solve the linearized scalar equation. For this purpose, the Kerr azimuthal coordinate φ^* and the tortoise coordinate x are introduced as

$$\begin{aligned} d\varphi^* &= d\varphi + \frac{a}{\Delta}dr, \\ dx &= \frac{r^2 + a^2}{\Delta}dr. \end{aligned} \tag{13}$$

Taking into account the axial symmetry of the KN background in Equation (5), the scalar perturbation could be decomposed as

$$\delta\phi(t, x, \theta, \varphi^*) = \sum_m \delta\phi(t, x, \theta)e^{im\varphi^*} \tag{14}$$

with m an azimuthal number. Substituting (14) into the linearized scalar Equation (9), we have the $(2+1)$-dimensional evolution equation

$$\begin{aligned}&\Big[-(r^2+a^2)^2+\Delta a^2\sin^2\theta\Big]\partial_t^2\delta\phi+(r^2+a^2)^2\partial_x^2\delta\phi+\Delta\partial_\theta^2\delta\phi\\&-2ima(r^2+a^2-\Delta)\partial_t\delta\phi+2\Big[r\Delta+ima(r^2+a^2)\Big]\partial_x\delta\phi+\Delta\cot\theta\partial_\theta\delta\phi\\&+\Delta\Big[-\mu_{\rm eff}^2(r^2+a^2\cos^2\theta)+\frac{m^2}{\sin^2\theta}\Big]\delta\phi=0.\end{aligned}\tag{15}$$

where the tortoise coordinate $x\in(-\infty,\infty)$ covers the whole region that is accessible to an observer located outside the outer horizon, while one confines the semi-infinite region $r\in[r_+,\infty)$ when using the coordinate r.

Considering the massive linearized scalar field, it may lead to instability or errors in numerical computations if directly applying the hyperboloidal slicing method. Here, we adopt the direct 2 + 1 time evolution method [24,25] to calculate the linearized massive scalar perturbation on the KN black hole background. The details on the code implementation were described in Ref. [27]. Here, we wish to mention the important things on how to solve Equation (15). The derivatives in x- and θ-directions are approximated by making use of a finite difference method, while the time evolution is carried out by adopting the fourth-order Runge–Kutta integrator. Moreover, we impose physical boundary conditions: an ingoing wave at the horizon and an outgoing wave at infinity. In practical calculations, one has to truncate the infinite radial computational domain to a finite range and put boundary conditions at the outer edges. It induces inevitably resulting spurious wave reflections from the outer edges. To overcome this "outer-boundary problem", one can push the outer edges to very large values so that the spurious reflections will not affect the observed signal for a sufficiently long evolution time. At the poles of $\theta=0$ and π, we impose the physical boundary condition of $\Psi|_{\theta=0,\pi}=0$ for $m\neq 0$, while $\partial_\theta\Psi|_{\theta=0,\pi}=0$ is imposed for $m=0$.

Importantly, the initial data of the scalar perturbation are chosen to be a Gaussian distribution localized outside the horizon with time symmetry as

$$\Psi(t=0,x,\theta)\sim P_m^l(\theta)e^{-\frac{(x-x_c)^2}{2\sigma^2}},\tag{16a}$$

$$\Pi(t=0,x,\theta)=0.\tag{16b}$$

where $P_m^l(\theta)$ denotes the associated Legendre polynomials, x_c represents a location of the center, and σ indicates a width of the distribution. It is worthy to point out that although there is one initial mode with a specified l only, other l modes with the same index m will be activated during the evolution. Hence, it is necessary to consider the influence of l and m of the initial perturbation. However, we note that the $l=m$ mode will have a dominant contribution at late times. To our knowledge, similar phenomena have occurred in other theories. Hereafter, we choose the initial mode Ψ with $l=m=0$ for simplicity.

4. Numerical Results

In this section, we describe schematic pictures concerning the influences of charge Q, spin a, coupling parameter α, and scalar mass m_ϕ on spin-charge-induced scalarization by solving the (2 + 1)-dimensional equation for a massive scalar. Before we proceed, we note that the Kerr spacetime is not spherically symmetric except when $a=0$, so the mode-coupling phenomenon occurs [19–21]: a pure initial l-multipole will excite other multipoles with the same m as it evolves. Taking into account this phenomenon and for simplicity, we consider $l=m=0$ mode for the KN black hole background.

Considering different values of coupling parameter α, the time domain profile of the $l = m = 0$-scalar mode $|\Psi|$ is shown in Figure 3. We note that $\alpha_{\rm th} = 24.4$ corresponds to the threshold (marginal) evolution of tachyonic instability for $m_\phi = 0.5$, $Q = 0.6$, and $a = 0.4$. From this figure, it is easily found that tachyonic instability is triggered once the coupling constant α exceeds $\alpha_{\rm th} = 24.4$. Similarly, Figure 4 indicates time-domain profiles of the scalar mode $|\Psi|$ with $m_\phi = 0.5$, $Q = 0.4$, and $a = 0.5$ for three couplings $\alpha = 66, 67$, and 68. Here, its threshold value is given by $\alpha_{\rm th} = 66.7$. We expect to find a similar time-domain profile of Ψ for the $Q = 0.2$ case. Actually, we note that $\alpha_{\rm th} = 24.4, 66.7$ can be predicted when finding its negative region of scalar potentials around the Kerr–Newman black hole. Qualitatively, the presence of the negative region for $\mu_{\rm eff}$ in Figures 1 ($\alpha = 24$) and 2 ($\alpha = 65$) implies that $\alpha_{\rm th}$ might take its values around $= 24$ and 65. However, the precise value of $\alpha_{\rm th}$ could be determined by observing the time-domain profile $|\Psi|$.

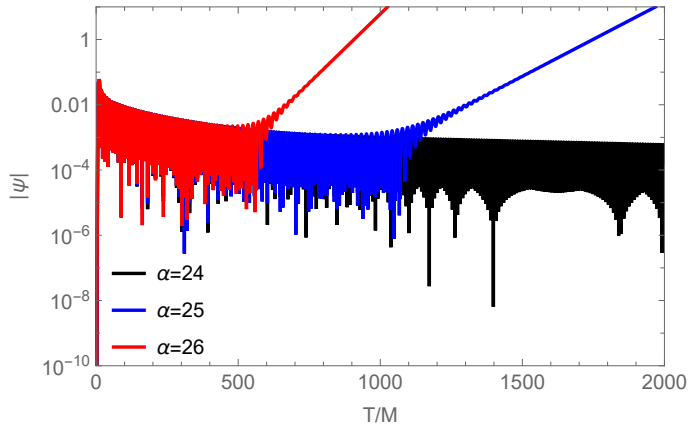

Figure 3. Time-domain profile of $|\Psi|$ for $m_\phi = 0.5$, $Q = 0.6$, and $a = 0.4$ with three coupling parameters $\alpha = 24, 25, 26$. Here, $\alpha = 24.4$ represents the threshold value ($\alpha_{\rm th}$). Hence, $\alpha = 25$ and 26 are unstable modes, while $\alpha = 24$ is a stable mode.

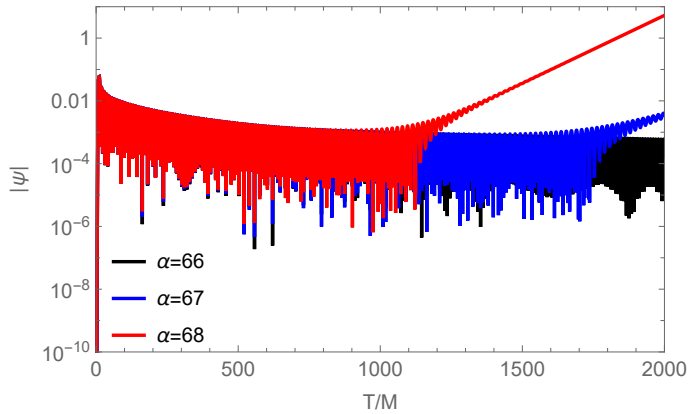

Figure 4. Time-domain profile of $|\Psi|$ for $m_\phi = 0.5$, $Q = 0.4$, and $a = 0.5$ with three couplings $\alpha = 66, 67, 68$. Here, $\alpha = 66.7$ represents the threshold value ($\alpha_{\rm th}$).

Importantly, we obtain the threshold curve $[\log_{10} \alpha_{\rm th}(a)]$ with different charge Q and scalar mass m_ϕ by making use of the $l = m = 0$-mode Ψ. A more clear picture for the influence of two parameters on the threshold curve is depicted in Figures 5 and 6. The threshold curve $\log_{10} \alpha_{\rm th}(a)$ describes the boundary between stable and unstable KN black holes. The allowed region for spin a is determined by its existence condition. The unstable region for scalarized KN black holes depends on the scalar mass.

The termination point of each curve determined by $\log_{10} \alpha_{\rm th}(a = 0, Q, m_\phi)$ increases as the scalar mass increases. For $m_\phi = 0$, the scalar becomes massless, and its unstable

region is the largest one when comparing with $m_\phi \neq 0$. Figure 7 shows that for given Q, three threshold curves are located from left to right as m_ϕ increases. The position of the termination point increases as the scalar mass increases. This confirms clearly that the presence of scalar mass suppresses or quenches the tachyonic instability in the KN spacetime [24,25]. Finally, considering the existence condition of the outer horizon Equation (8) with $M = 1$, one may determine the upper bound of a. For $Q = 0.2,\ 0.4$, and 0.6, the maximum values (upper bounds) of a are given by 0.980, 0.917, and 0.8, respectively (see Figures 1, 2 and 5–7).

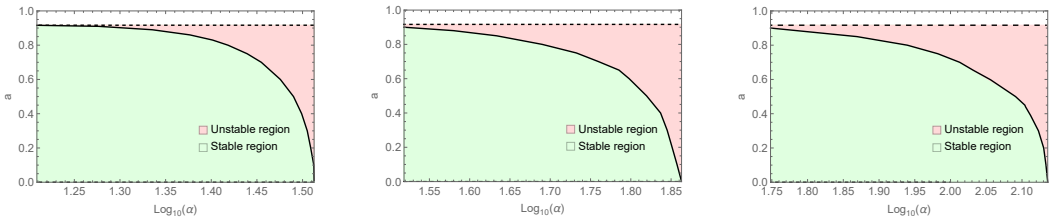

(**a**) $m_\phi = 0$ (**b**) $m_\phi = 0.5$ (**c**) $m_\phi = 1$

Figure 5. Threshold curves $\log_{10} \alpha_{\rm th}(a)$ for $Q = 0.4$ with different scalar mass $m_\phi = 0,\ 0.5,\ 1$. All curves denote the boundaries between stable (lower) and unstable (upper) region. Black solid lines represent the existence condition $[a^2 \leq 1 - Q^2 (= 0.84)]$ of the outer horizon.

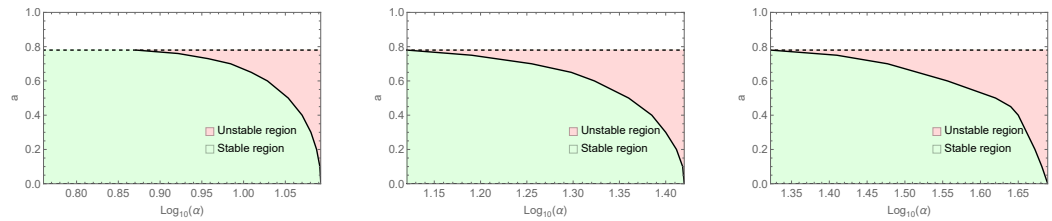

(**a**) $m_\phi = 0$ (**b**) $m_\phi = 0.5$ (**c**) $m_\phi = 1$

Figure 6. Threshold curves $\log_{10} \alpha_{\rm th}(a)$ for $Q = 0.6$ with three scalar mass $m_\phi = 0,\ 0.5,\ 1$. All curves denote the boundaries between stable (lower) and unstable (upper) region. Black solid lines represent the existence condition $[a^2 \leq 1 - Q^2 (= 0.64)]$ of the outer horizon.

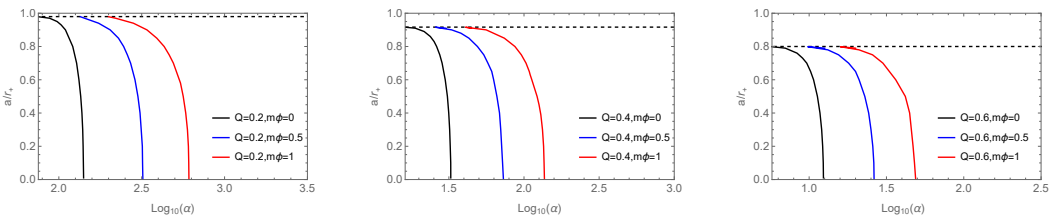

Figure 7. Threshold curves $\log_{10} \alpha_{\rm th}(a)$ for three charges $Q = 0.2,\ 0.4,\ 0.6$ with three scalar masses $m_\phi = 0,\ 0.5,\ 1$. All curves denote the boundaries between the stable and unstable region. Black solid lines determine the existence condition $a^2(Q) \leq 1 - Q^2$ of the outer horizon.

5. Conclusions and Discussions

In this work, we have analyzed the spin-charge-induced scalarization of KN black holes described by mass $M = 1$, charge Q, and spin a in the EMS theory with scalar mass m_ϕ and positive scalar coupling $\alpha > 0$. We found that there exists a bound of $0 < a < a_o$ with onset spin $a_o(Q, m_\phi, \alpha)$ for the negative region signaling instability by analyzing the effective scalar mass term $\mu^2_{\rm eff}$ in the θ-direction. However, it implies that as a whole, there is no spin-bound on the onset of scalarization with positive coupling parameter α because the contribution of $\mu^2_{\rm eff}$ around $(\theta = \pi/2)$ is dominant negatively. We adopted the fourth-order Runge–Kutta integrator to solve the $(2+1)$-dimensional evolution equation. We have

obtained the threshold curves [$\log_{10} \alpha_{\rm th}(a, Q, m_\phi)$] to describe boundaries between stable (lower region) and unstable (upper region) KN black holes. Moreover, all threshold curves increase as a decreases with the upper bound determined by $a^2 \leq 1 - Q^2$. The unstable region is allowed only for constructing scalarized KN black holes.

Finally, the computation including nonlinear effects is expected to quench the tachyonic instability and leads to constructing scalarized KN black holes. Hence, a promising direction is to construct the scalarized KN black holes in the EMS theory with positive scalar coupling and mass term.

Author Contributions: Conceptualization, M.-Y.L., Y.S.M., Y.-B.H. and D.-C.Z.; Methodology, X.L., M.-Y.L., Y.S.M. and D.-C.Z.; Software, X.L. and Y.S.M.; Validation, Y.S.M. and D.-C.Z.; Formal analysis, X.L. and Y.S.M.; Investigation, Y.S.M.; Resources, X.L., M.-Y.L., Y.S.M. and D.-C.Z.; Data curation, X.L. and Y.S.M.; Writing—original draft, M.-Y.L., Y.S.M. and D.-C.Z.; Writing—review & editing, Y.S.M. and D.-C.Z.; Visualization, X.L., Y.S.M. and D.-C.Z.; Supervision, M.-Y.L., Y.S.M., Y.-B.H. and D.-C.Z.; Project administration, D.-C.Z.; Funding acquisition, D.-C.Z. All authors have read and agreed to the published version of the manuscript.

Funding: This research was funded by Natural Science Foundation of China (NNSFC) (Grant No. 12365009 and 12305064).

Data Availability Statement: The original contributions presented in this study are included in the article.

Acknowledgments: We appreciate Xu Yang for helpful discussion.

Conflicts of Interest: The authors declare no conflict of interest.

References

1. Carter, B. Axisymmetric Black Hole Has Only Two Degrees of Freedom. *Phys. Rev. Lett.* **1971**, *26*, 331–333. [CrossRef]
2. Ruffini, R.; Wheeler, J.A. Introducing the black hole. *Phys. Today* **1971**, *24*, 30. [CrossRef]
3. Bekenstein, J.D. Exact solutions of Einstein conformal scalar equations. *Ann. Phys.* **1974**, *82*, 535. [CrossRef]
4. Bekenstein, J.D. Black Holes with Scalar Charge. *Ann. Phys.* **1975**, *91*, 75. [CrossRef]
5. Bronnikov, K.A.; Kireev, Y.N. Instability of Black Holes with Scalar Charge. *Phys. Lett. A* **1978**, *67*, 95. [CrossRef]
6. Damour, T.; Esposito-Farese, G. Nonperturbative strong field effects in tensor–scalar theories of gravitation. *Phys. Rev. Lett.* **1993**, *70*, 2220–2223. [CrossRef]
7. Doneva, D.D.; Yazadjiev, S.S. New Gauss-Bonnet Black Holes with Curvature-Induced Scalarization in Extended Scalar-Tensor Theories. *Phys. Rev. Lett.* **2018**, *120*, 131103. [CrossRef]
8. Silva, H.O.; Sakstein, J.; Gualtieri, L.; Sotiriou, T.P.; Berti, E. Spontaneous scalarization of black holes and compact stars from a Gauss-Bonnet coupling. *Phys. Rev. Lett.* **2018**, *120*, 131104. [CrossRef]
9. Antoniou, G.; Bakopoulos, A.; Kanti, P. Evasion of No-Hair Theorems and Novel Black-Hole Solutions in Gauss-Bonnet Theories. *Phys. Rev. Lett.* **2018**, *120*, 131102. [CrossRef]
10. Fernandes, P.G.S.; Herdeiro, C.A.R.; Pombo, A.M.; Radu, E.; Sanchis-Gual, N. Spontaneous Scalarisation of Charged Black Holes: Coupling Dependence and Dynamical Features. *Class. Quant. Grav.* **2019**, *36*, 134002. Erratum in *Class. Quant. Grav.* **2020**, *37*, 049501. [CrossRef]
11. Herdeiro, C.A.R.; Radu, E. Black hole scalarization from the breakdown of scale invariance. *Phys. Rev. D* **2019**, *99*, 084039. [CrossRef]
12. Herdeiro, C.A.R.; Radu, E.; Sanchis-Gual, N.; Font, J.A. Spontaneous Scalarization of Charged Black Holes. *Phys. Rev. Lett.* **2018**, *121*, 101102. [CrossRef] [PubMed]
13. Myung, Y.S.; Zou, D.C. Instability of Reissner–Nordström black hole in Einstein-Maxwell-scalar theory. *Eur. Phys. J. C* **2019**, *79*, 273. [CrossRef]
14. Hod, S. Onset of spontaneous scalarization in spinning Gauss-Bonnet black holes. *Phys. Rev. D* **2020**, *102*, 084060. [CrossRef]
15. Zhang, S.J.; Wang, B.; Wang, A.; Saavedra, J.F. Object picture of scalar field perturbation on Kerr black hole in scalar-Einstein-Gauss-Bonnet theory. *Phys. Rev. D* **2020**, *102*, 124056. [CrossRef]
16. Doneva, D.D.; Collodel, L.G.; Krüger, C.J.; Yazadjiev, S.S. Black hole scalarization induced by the spin: 2+1 time evolution. *Phys. Rev. D* **2020**, *102*, 104027. [CrossRef]

17. Berti, E.; Collodel, L.G.; Kleihaus, B.; Kunz, J. Spin-induced black-hole scalarization in Einstein-scalar-Gauss-Bonnet theory. *Phys. Rev. Lett.* **2021**, *126*, 011104. [CrossRef]
18. Dima, A.; Barausse, E.; Franchini, N.; Sotiriou, T.P. Spin-induced black hole spontaneous scalarization. *Phys. Rev. Lett.* **2020**, *125*, 231101. [CrossRef]
19. Cunha, P.V.P.; Herdeiro, C.A.R.; Radu, E. Spontaneously Scalarized Kerr Black Holes in Extended Scalar-Tensor–Gauss-Bonnet Gravity. *Phys. Rev. Lett.* **2019**, *123*, 011101. [CrossRef]
20. Collodel, L.G.; Kleihaus, B.; Kunz, J.; Berti, E. Spinning and excited black holes in Einstein-scalar-Gauss–Bonnet theory. *Class. Quant. Grav.* **2020**, *37*, 075018. [CrossRef]
21. Herdeiro, C.A.R.; Radu, E.; Silva, H.O.; Sotiriou, T.P.; Yunes, N. Spin-induced scalarized black holes. *Phys. Rev. Lett.* **2021**, *126*, 011103. [CrossRef] [PubMed]
22. Zou, D.C.; Myung, Y.S. Rotating scalarized black holes in scalar couplings to two topological terms. *Phys. Lett. B* **2021**, *820*, 136545 [CrossRef]
23. Doneva, D.D.; Collodel, L.G.; Yazadjiev, S.S. Spontaneous nonlinear scalarization of Kerr black holes. *Phys. Rev. D* **2022**, *106*, 104027. [CrossRef]
24. Doneva, D.D.; Collodel, L.G.; Krüger, C.J.; Yazadjiev, S.S. Spin-induced scalarization of Kerr black holes with a massive scalar field. *Eur. Phys. J. C* **2020**, *80*, 1205. [CrossRef]
25. Zhang, S.J. Massive scalar field perturbation on Kerr black holes in dynamical Chern–Simons gravity. *Eur. Phys. J. C* **2021**, *81*, 441. [CrossRef]
26. Hod, S. Spin-charge induced scalarization of Kerr-Newman black-hole spacetimes. *J. High Energy Phys.* **2022**, *2022*, 272. [CrossRef]
27. Lai, M.Y.; Myung, Y.S.; Yue, R.H.; Zou, D.C. Spin-induced scalarization of Kerr-Newman black holes in Einstein-Maxwell-scalar theory. *Phys. Rev. D* **2022**, *106*, 044045. [CrossRef]
28. Zenginoglu, A. Hyperboloidal foliations and scri-fixing. *Class. Quant. Grav.* **2008**, *25*, 145002. [CrossRef]
29. Lai, M.Y.; Myung, Y.S.; Yue, R.H.; Zou, D.C. Spin-charge induced spontaneous scalarization of Kerr-Newman black holes. *Phys. Rev. D* **2022**, *106*, 084043. [CrossRef]
30. Zou, D.C.; Myung, Y.S. Scalarized charged black holes with scalar mass term. *Phys. Rev. D* **2019**, *100*, 124055. [CrossRef]

Disclaimer/Publisher's Note: The statements, opinions and data contained in all publications are solely those of the individual author(s) and contributor(s) and not of MDPI and/or the editor(s). MDPI and/or the editor(s) disclaim responsibility for any injury to people or property resulting from any ideas, methods, instructions or products referred to in the content.